Electronic Supplementary Material (ESI) for Inorganic Chemistry Frontiers.

Electronic Supplementary Information

Noncovalent induced circular dichroism sensor based on chiral metal-organic framework: chiral induction synthesis, quantitative enantioselective sensing and noncovalent sensing mechanism

Yanyu Zhu, Tianyang Ding, Xu Zhang, Yanan Zhou, Jiahui Yu, Xin Li, Hanwen Zheng, Zhengang Sun* and Chengqi Jiao*

School of Chemistry and Chemical Engineering, Liaoning Normal University, Dalian 116029, China.

Email: szg188@163.com, jiaochengqi1989@163.com

Contents **Page**

1. Experimental section

Materials and measurements. $HOOCC_6H_4CH_2PO(OH)(OC_2H_5)$ (H_2L) was prepared according to the procedures described previously.[1] All other chemical reagent were acquired from a professional institution without further purification. Powder X-ray diffraction (PXRD) patterns were recorded on a Bruker D8 Advance diffractometer with Cu–Kα radiation (λ = 1.5418 Å). Elemental analyses of C, H and N were carried out on the PE–2400 elemental analyzer. The elemental content of Zn^{II} and Cu^{II} ions was measured by inductively coupled plasma emission spectrometry (ICP). Thermal gravimetric (TG) analysis was obtained on a Perkin–Elmer Pyris Diamond TG–DTA thermal analyzer under static air with a heating rate of 10 K min^{-1}. Fourier transform infrared (FT–IR) spectra were recorded on a Bruker AXS TENSOR–27 FT–IR spectrometer with KBr pellets in the range 4000~400 cm^{-1}. CD spectra of the solid state and aqueous suspensions were recorded on a MOS–500 (Bio–Logic, France) spectropolarimeter at room temperature. In the measurement of solid-state CD spectra, a mixture of 1 mg bulk sample (or 1 big single crystal) and 20 mg dried KBr powder was well-ground and pressed into a disk.

Synthesis of [Cu(L)(2,2'-bipy)]·H_2O (LNNU-2), (*M*)-LNNU-2 and (*P*)-LNNU-2. A mixture of $Cu(CH_3COO)_2·H_2O$ (0.50 mmol, 0.100 g), H_2L (0.25 mmol, 0.061 g), 2,2'-bipy (0.45 mmol, 0.070 g) and deionized water (10 mL) was stirred for 60 min, and then sealed in a 20 mL Teflon-lined stainless autoclave at 80°C for 3 days. After it was cooled to ambient temperature, the blue block crystals were obtained. Yield: 0.0515 g, 42.9% (based on H_2L). Elemental analysis calcd (%) for $C_{20}H_{21}N_2O_6PCu$: C, 50.06; H, 4.41; N, 5.84; found: C, 50.11; H, 4.45; N, 5.88. The synthetic procedure of **(*M*)-LNNU-2** was the same as that for **LNNU-2** except that the deionized water was replaced by an aqueous solution of D-Ala (2.5×10^{-3} M, 10 mL). Blue block crystals of **(*M*)-LNNU-2** were obtained and washed with water. Yield: 0.0717 g, 59.8% (based on H_2L). The synthetic procedure of **(*P*)-LNNU-2** was the same as that for **LNNU-2** except that the deionized water was replaced by an aqueous solution of L-Ala (2.5×10^{-3} M, 10 mL). Blue block crystals of **(*P*)-LNNU-2** were obtained and washed with water. Yield: 0.0535 g, 44.6% (based on H_2L).

Synthesis of [Zn_xCu_y(L)(2,2'-bipy)]·H_2O (x: y = 9.6: 0.4~1.0: 9.0). A mixture of metal salts (0.50 mmol), H_2L (0.30 mmol, 0.073 g), 2,2'-bipy (0.45 mmol, 0.070 g) and deionized water (10 mL) was stirred for 60 min, and then sealed in a 20 mL Teflon-lined stainless autoclave at 80°C for 3 days. After it was cooled to ambient temperature, the blue block crystals of 9 kinds of bimetallic MOFs with

different Zn^{II}/Cu^{II} ratios were obtained. The amount of raw materials of $Zn(CH_3COO)_2{\cdot}2H_2O$ and $Cu(CH_3COO)_2{\cdot}H_2O$, the actual molar ratios of Zn^{II}/Cu^{II} in the bimetallic MOFs, and the yields are shown in Table S3.

Synthesis of [Cd(L)(2,2'-bipy)(H_2O)] (LNNU-3). A mixture of $Cd(CH_3COO)_2{\cdot}2H_2O$ (0.50 mmol, 0.133 g), H_2L (0.25 mmol, 0.061 g), 2,2'-bipy (0.45 mmol, 0.070 g) and deionized water (10 mL) was stirred for 60 min, and then sealed in a 20 mL Teflon-lined stainless autoclave at 160°C for 3 days. After it was cooled to ambient temperature, the colorless block crystals were obtained. Yield: 0.0675g, 51.1% (based on H_2L). Elemental analysis calcd (%) for $C_{20}H_{21}N_2O_6PCd$: C, 45.43; H, 4.00; N, 5.30; found: C, 45.48; H, 4.05; N 5.34.

Crystallographic studies. X-ray diffraction data for **(*M*)-LNNU-2**, **(*P*)-LNNU-2** and **LNNU-3** were collected on a Bruker AXS Smart APEX II CCD X–diffractometer with graphite-monochromated Mo–Kα (λ = 0.71073 Å). The structures were solved by direct methods and refined on F^2 by full-matrix least-squares methods by using SHELXL-2014/7.[2] All non-hydrogen atoms were refined anisotropically. H atoms of organic ligands were refined isotropically as a riding mode. Details of crystallographic data of **(*M*)-LNNU-2**, **LNNU-3** and **(*P*)-LNNU-2** are provided in Tables S1, S5 and S10, and corresponding bond lengths and angles are listed in Tables S2, S6 and S11, respectively.

Determination of L-Trp concentration. The CD spectra of the aqueous suspensions were collected in a continuous scanning mode, using a quartz cuvette (1 cm path length). The powder of **LNNU-2** (2.0 mg) was immersed in deionized water (2.0 mL) to form the suspension after treating by ultrasonication for 20 min. Then, the CD titration experiments were performed by stepwise addition of L-Trp aqueous solution (2.5×10^{-3} M) into the aqueous suspension of **LNNU-2**. After each addition, the CD spectrum of the suspension was monitored. All the experiments were repeated three times to obtain reliable average values. Each of 19 natural amino acids except L-Trp was prepared as 2.0×10^{-3} M aqueous solution, and the aqueous solutions of the above natural amino acids were mixed in equal volume. 2 mg powder of **LNNU-2** was immersed in 2.0 mL of the above aqueous solution of 19 natural amine mixture and then sonicated for 20 min. Similarly, the aqueous solutions of 8 typical substances in blood plasma (urea, glucose, $MgCl_2$, L-proline, $CaCl_2$, $NaHCO_3$, NaCl and KCl) were mixed in equal volume, and the concentration of each typical substance aqueous solution is 2.5×10^{-3} M. The powder of **LNNU-2** (2.0 mg) was immersed in the above mixed aqueous solution (2.0 mL) to form the

suspension after treating by ultrasonication for 20 min. The CD titration experiments in the mixed natural amino acids and blood plasma components were performed in the same way as in water.

Determination of the absolute configuration and enantiomeric excess (*ee*) of chiral analytes. A calibration curve was constructed using samples containing Trp with varying enantiomeric composition in water. **LNNU-2** (2 mg) was immersed in an aqueous Trp solution (2.5×10^{-4} M, 3 mL) with varying *ee* (+100, +80, +60, +40, +20, 0, −20, −40, −60, −80 and −100%). CD analysis was conducted following ultrasonication for 20 min. The ICD signals at 325 nm directly correspond to the enantiomeric composition of Trp. The above experiment was conducted 3 times and the average value of the ICD signal intensity at 325 nm was calculated. The linear regression equation calculated from the calibration curve that determined by average values of ICD signal intensity plotted against *ee* values of Trp samples. Two calibration curves were constructed using samples containing two chiral aromatic amino alcohols (2-phenylglycinol (**1**) and (-)-cis-1-amino-2-indanol (**2**)) with varying enantiomeric composition in water, respectively. **LNNU-2** (2.0 mg) was dispersed in aqueous solutions (3.0×10^{-3} M, 3.0 mL) of the two chiral aromatic amino alcohols with varying *ee* (+100, +80, +60, +40, +20, 0, −20, −40, −60, −80 and −100%), respectively. CD analysis was conducted following ultrasonication for 20 min. The average values of the ICD signal intensities at 565 nm for **1** and 603 nm for **2** were calculated, respectively. The linear regression equations calculated from the calibration curves that determined by average values of ICD signal intensities plotted against *ee* of chiral aromatic amino alcohol samples.

2. Noncovalent interactions between LNNU-1 and chiral Trp

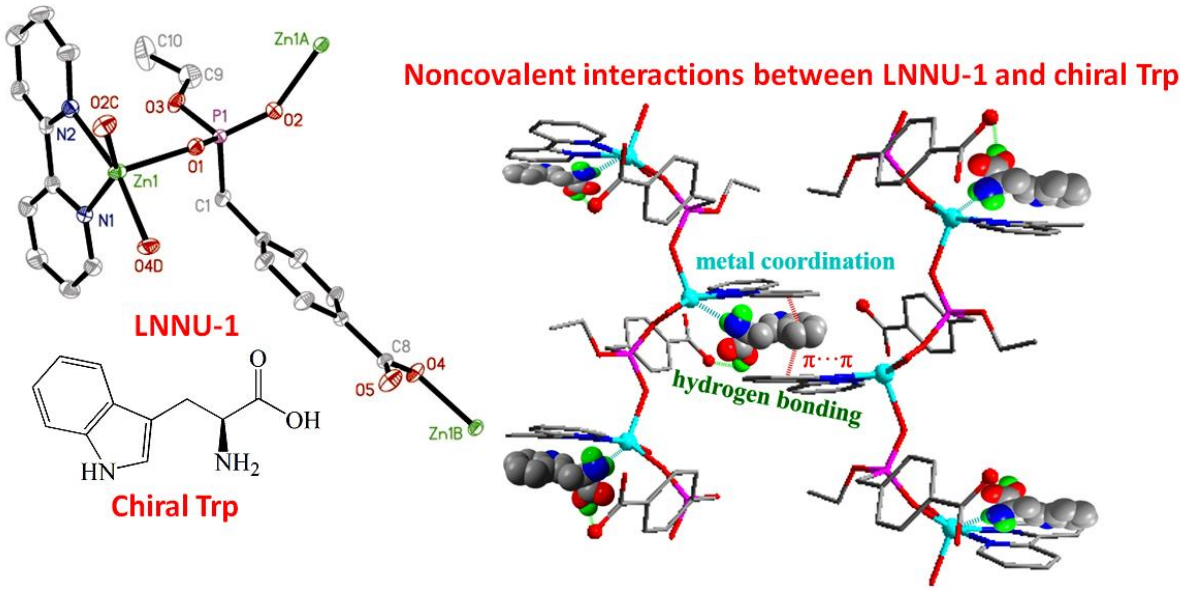

Fig. S1 Schematic diagram of noncovalent interactions between **LNNU-1** and chiral Trp.[3]

3. Crystal structure of LNNU-2

LNNU-2 crystallized in chiral space group of $P2_12_12_1$, and the Flack absolute configuration parameter (0.029(4)) further verified the chirality (Table S1).[4] Single-crystal structural analysis indicated the central Cu^{II} ion adopted a five-coordinated distorted square pyramidal geometry surrounded by two phosphonate oxygen atoms (O1 and O2C) and one carboxylate oxygen atom (O4D) from three separate L^{2-} anions, as well as two nitrogen atoms (N1 and N2) from one 2,2'-bipy molecule (Fig. S2a). The evaluation of the crystal structure of **LNNU-2** revealed two pyridyl rings in 2,2'-bipy are not coplanar with the dihedral angle was 7.77° (Fig. S2a). Thus, the axial chirality of 2,2'-bipy is an important element of chirality in **LNNU-2**. It could be seen that the crystal structure of **LNNU-2** was the same as that of **LNNU-1**, and had an unsaturated coordination metal center, which could be used as a Lewis acidic site for the sensing of chiral Trp. As demonstrated in Fig. S2b, the $\{CuN_2O_3\}$ square pyramids and the $\{CPO_3\}$ tetrahedra were interconnected into a left-handed helical (*M*-helical) chain running along the *b*-axis. Additionally, the helix chains were bridged by the carboxylate moieties of the L^{2-} ligands to form a 2D network in the *ab*-plane. Stacking of the 2D layers could be observed when viewing the structure along the *a*-axis (Fig. S2c). The distance of the interlayer was

approximately 10.192(9) Å. The non-coordinated carboxyl oxygen (O5) atom of the L^{2-} ligand was orientated toward the interlayer space, which could offer a potential site for molecular sensing by hydrogen bonding interactions. It was also noteworthy that the pyridyl rings in the interlayer space could provide effective sites for molecular sensing by exhibiting aromatic stacking interactions. Crystal structure analysis indicated **LNNU-2** and **LNNU-1** had the same functional sites except for the different Lewis acidity of the central metal. Therefore, **LNNU-1** and **LNNU-2** could be used to study the effects of metal coordination interaction on the generation and amplification of ICD signals in the noncovalent ICD sensing system.

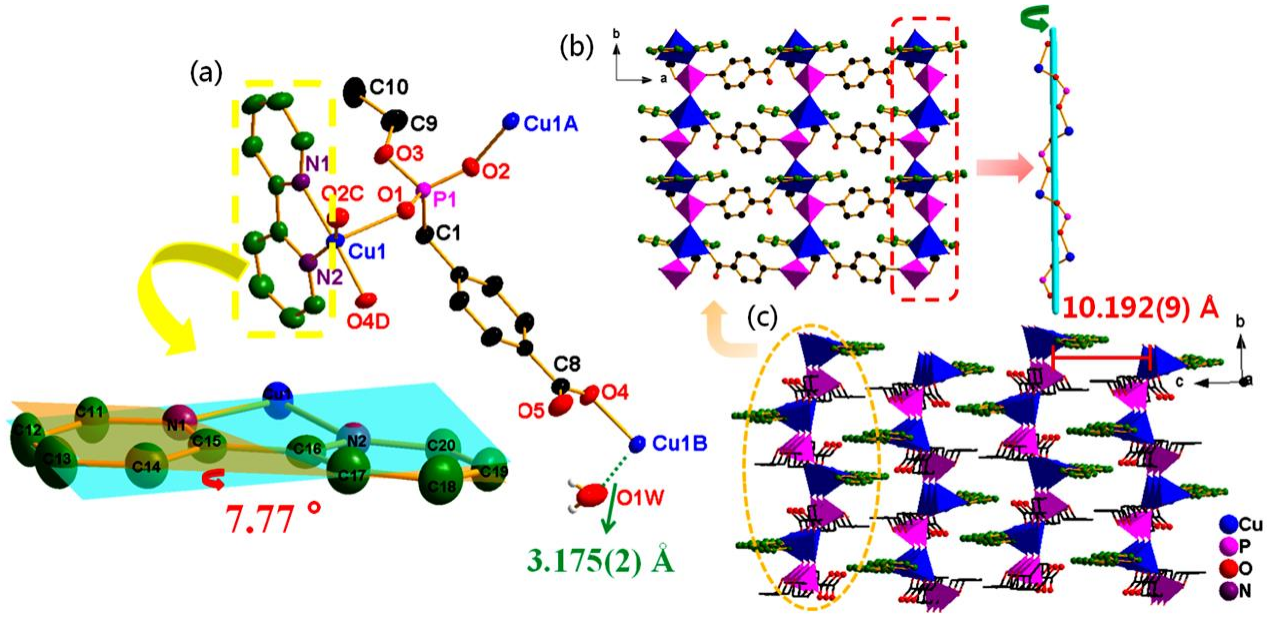

Fig. S2 (a) The structure unit of **LNNU-2** showing the atom labeling and the angle between two pyridine rings in the axially chiral conformation of 2,2'-bipy; (b) The 2D network of **LNNU-2** with a left-handed helical chain running along the *b*-axis; (c) Layer structure of **LNNU-2** viewed along *a*-axis. The colour of carbon atoms in the L^{2-} ligand and pyridyl rings are black and green, respectively.

Table S1 Crystal data and structure refinement for **LNNU-2**

Formula	$C_{20}H_{21}N_2O_6PCu$
Fw	479.90
Crystal size (mm)	0.176 × 0.094 × 0.082
Crystal system	Orthorhombic
Space group	$P2_12_12_1$
a (Å)	10.0840(4)
b (Å)	10.9173(4)
c (Å)	18.4068(7)
V (Å^3)	2026.41(13)
Z	4
D_c (g cm^{-3})	1.573
μ (mm^{-1})	1.198
F (000)	988
GOF on F^2	1.032
Unique date, R_{int}	4172, 0.0170
Theta range (º)	2.169 to 26.489
R_1, wR_2 [a)] (for $I>2\sigma(I)$)	0.0216, 0.0593
R_1, wR_2 [a)] (for all data)	0.0237, 0.0602
$\Delta\rho_{max}$, $\Delta\rho_{min}$ (e Å^{-3})	0.234, –0.279
Flack parameter	0.029(4)
Absolute configuration	*M*
CCDC number	1964191

[a)] $R_1 = \Sigma(||F_0|-|F_C||) / \Sigma|F_0|$; $wR_2 = [\Sigma w(|F_0|-|F_C|)^2 / \Sigma w F_0^2]^{1/2}$

Table S2 Selected bond lengths (Å) and angles (º) for **LNNU-2**

Bond lengths (Å)			
Cu(1)–O(1)	2.2855(17)	P(1)–O(1)	1.4932(18)
Cu(1)–O(2)#1	1.9358(19)	P(1)–O(2)	1.5018(18)
Cu(1)–O(4)#2	1.9448(18)	P(1)–O(3)	1.5927(19)
Cu(1)–N(1)	2.014(2)	P(1)–C(1)	1.812(3)
Cu(1)–N(2)	2.045(2)	O(3)–C(9)	1.448(4)
C(9)–C(10)	1.442(10)	O(4)–C(8)	1.281(3)
O(5)–C(8)	1.235(3)		
Bond angles (º)			
O(2)#1–Cu(1)–O(4)#2	94.25(9)	O(1)–P(1)–O(2)	118.09(11)
O(2)#1–Cu(1)–O(1)	96.68(7)	O(2)–P(1)–O(3)	110.57(11)
O(4)#2–Cu(1)–O(1)	90.06(8)	O(1)–P(1)–O(3)	106.79(11)
O(2)#1–Cu(1)–N(1)	89.91(9)	O(1)–P(1)–C(1)	110.85(12)
O(4)#2–Cu(1)–N(1)	175.38(9)	O(2)–P(1)–C(1)	106.11(12)
O(1)–Cu(1)–N(1)	91.45(8)	O(3)–P(1)–C(1)	103.51(11)
N(1)–Cu(1)–N(2)	79.89(9)	C(9)–O(3)–P(1)	120.7(2)
O(2)#1–Cu(1)–N(2)	160.27(9)	P(1)–O(1)–Cu(1)	133.86(10)
O(4)#2–Cu(1)–N(2)	95.54(9)	C(15)–N(1)–Cu(1)	115.68(19)
O(1)–Cu(1)–N(2)	100.39(8)	C(20)–N(2)–Cu(1)	126.77(19)

Symmetry codes: #1 –x, y – 1/2, –z + 1/2; #2 –x + 1, y – 1/2, –z + 1/2.

4. Characterization of bimetallic MOFs

Table S3 Synthesis conditions of a series of bimetallic MOFs

Reactant Zn^{II}/Cu^{II} ratio	$Zn(OAc)_2 \cdot 2H_2O$ (mmol)	$Cu(OAc)_2 \cdot H_2O$ (mmol)	Yield (based on H_2L) %	ICP Results Zn^{II}/Cu^{II} ratio
9.0: 1.0	0.45	0.05	41.5	9.6: 0.4
8.0: 2.0	0.40	0.10	50.2	9.2: 0.8
7.0: 3.0	0.35	0.15	40.9	8.5: 1.5
6.0: 4.0	0.30	0.20	51.3	7.5: 2.5
5.0: 5.0	0.25	0.25	36.9	6.6: 3.4
4.0: 6.0	0.20	0.30	44.5	5.7: 4.3
3.0: 7.0	0.15	0.35	34.7	4.2: 5.8
2.0: 8.0	0.10	0.40	43.8	2.5: 7.5
1.0: 9.0	0.05	0.45	54.1	1.0: 9.0

5. Structural Stabilities of LNNU-2 and Bimetallic MOFs

LNNU-2 and bimetallic MOFs had similar thermal gravimetric (TG) curves, thus, **LNNU-2** was used as an example to illuminate the weight losses in detail (Fig. S3a and b). The TG curve of **LNNU-2** exhibited three main steps of weight loss. The first step started at 157 °C and was completed at 200 °C, corresponding to the release of one lattice water molecule. The observed weight loss of 3.5% was a little less than the calculated value (3.8%). The release of the lattice water molecule up to a high temperature was rare. As shown in Fig. S2, the distance between the lattice water (O1W) and the central Cu^{II} ion was 3.175(2) Å, indicating a possible secondary bonding interaction between them. This might be the reason for the loss of the lattice water at the high temperature. The PXRD patterns and FT-IR spectra of the heated samples demonstrated that the framework structure of **LNNU-2** was still stable at 200°C (Fig. S3c and d). The above results indicated that the thermal stability of **LNNU-2** was higher than that of **LNNU-1**. The second step between 240 °C and 345 °C could be attributed to the partial decomposition of the organic moieties. Up to this temperature, a complicated weight loss occurred until 730 °C, which corresponded to further decomposition of the organic moieties. The total weight loss observed was 70.1%.

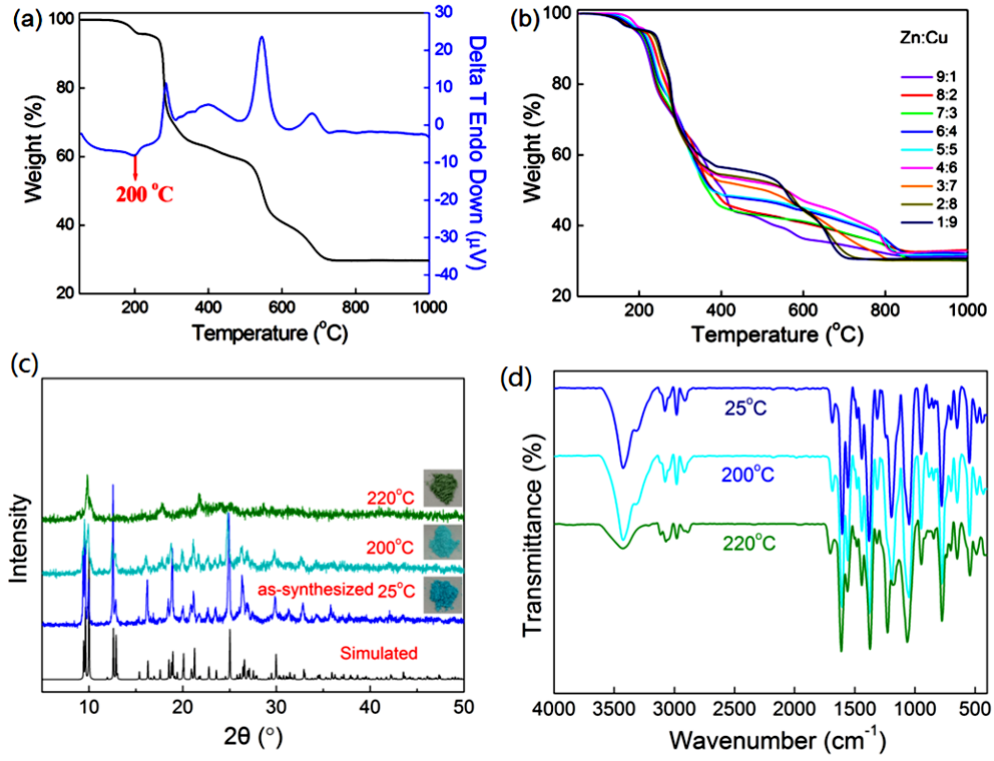

Fig. S3 (a) TG–DTA curves of **LNNU-2**; (b) TG curves of the bimetallic MOFs; (c) The variable temperature PXRD patterns and (d) FT–IR spectra of **LNNU-2** in the range of 25~220 °C.

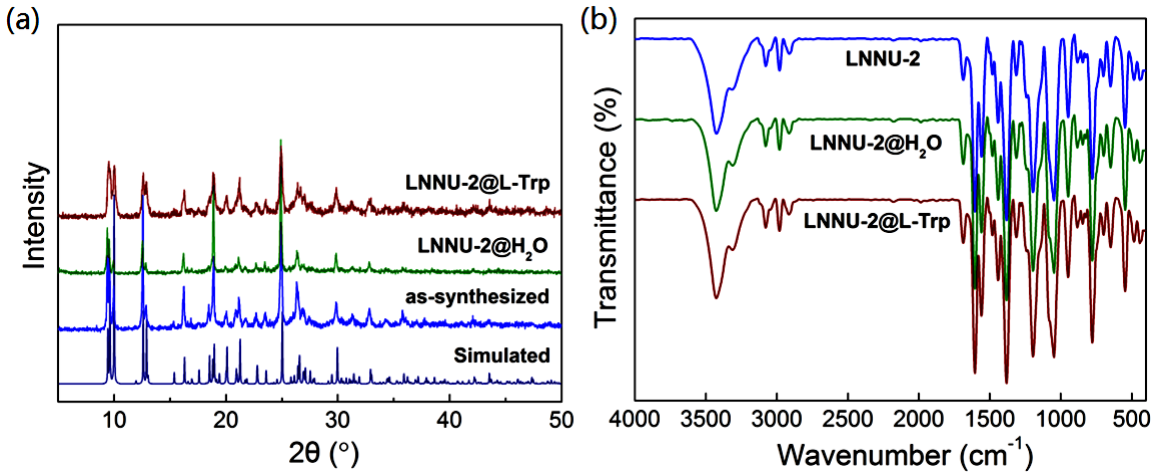

Fig. S4 (a) PXRD patterns and (b) FT–IR spectra of **LNNU-2** immersed in pure water and aqueous solution of L-Trp (2.5×10^{-3} M) for 6 h, respectively.

6. ICD signals of MOF@L-Trp suspensions

Table S4 Peak position and intensity of ICD signal of MOF@L-Trp suspension

MOF@L-Trp suspension Zn^{II}/Cu^{II} ratio	ICD signal peak position (nm)	ICD signal Intensity (mdeg)
10.0: 0.0 (**LNNU-1**)	319	26.4
9.6: 0.4	320	32.2
9.2: 0.8	321	36.6
8.5: 1.5	321	41.4
7.5: 2.5	321	53.2
6.6: 3.4	322	63.1
5.7: 4.3	322	74.1
4.2: 5.8	324	104.0
2.5: 7.5	325	113.6
1.0: 9.0	327	123.3
0.0: 10.0 (**LNNU-2**)	329	152.5

7. Crystal structure, characterization and stability studies of LNNU-3

LNNU-3 was successfully synthesized by replacing the central Zn^{II} ions of **LNNU-1** with the Cd^{II} ions. The crystal structure of **LNNU-3** was characterized by single crystal X-ray diffraction, PXRD and FT–IR spectroscopy (Fig. S5, S6a and b). The framework structure of **LNNU-3** was similar to that of **LNNU-1** except that the central Cd^{II} ion was six-coordinated and the coordinated water molecule (O6) occupied the unsaturated site of the metal center (Fig. S5, Table S5 and S6). The thermal weight loss process of **LNNU-3** was similar to that of **LNNU-2** (Fig. S6c), so it would not be discussed in detail. **LNNU-3** also crystallized in chiral space group of $P2_12_12_1$ with a Flack absolute configuration parameter close to zero (0.000(9)), indicating the enantiomeric purity of the single crystal (Table S5).[4] Since the single crystal size of **LNNU-3** was too small, the solid-state CD spectrum of the single-crystal sample could not be obtained, the solid-state CD spectra of 10 bulk samples of **LNNU-3** randomly picked from the same batch were measured. As shown in Fig. S6d, all CD spectra showed the same Cotton effects, indicating that the bulk sample of **LNNU-3** was also chiral.

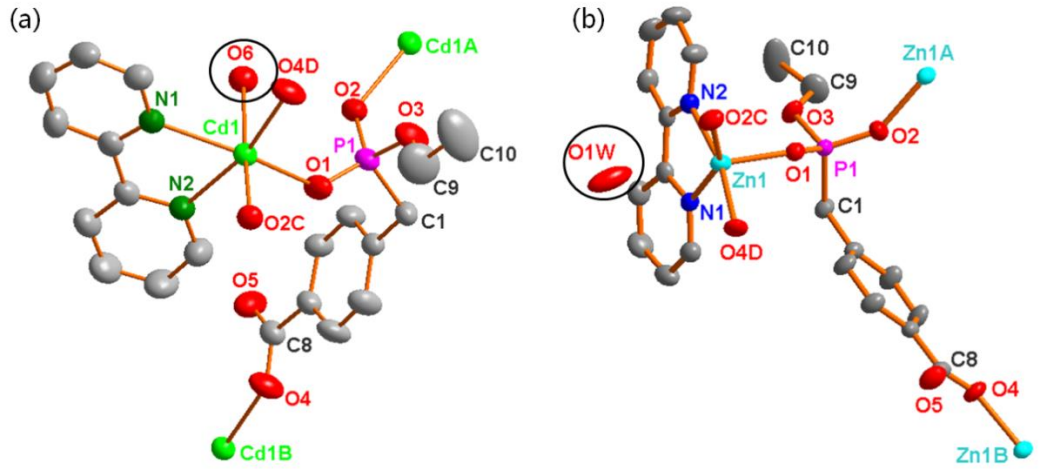

Fig. S5 Crystal structures of **LNNU-3** (a) and **LNNU-1** (b).

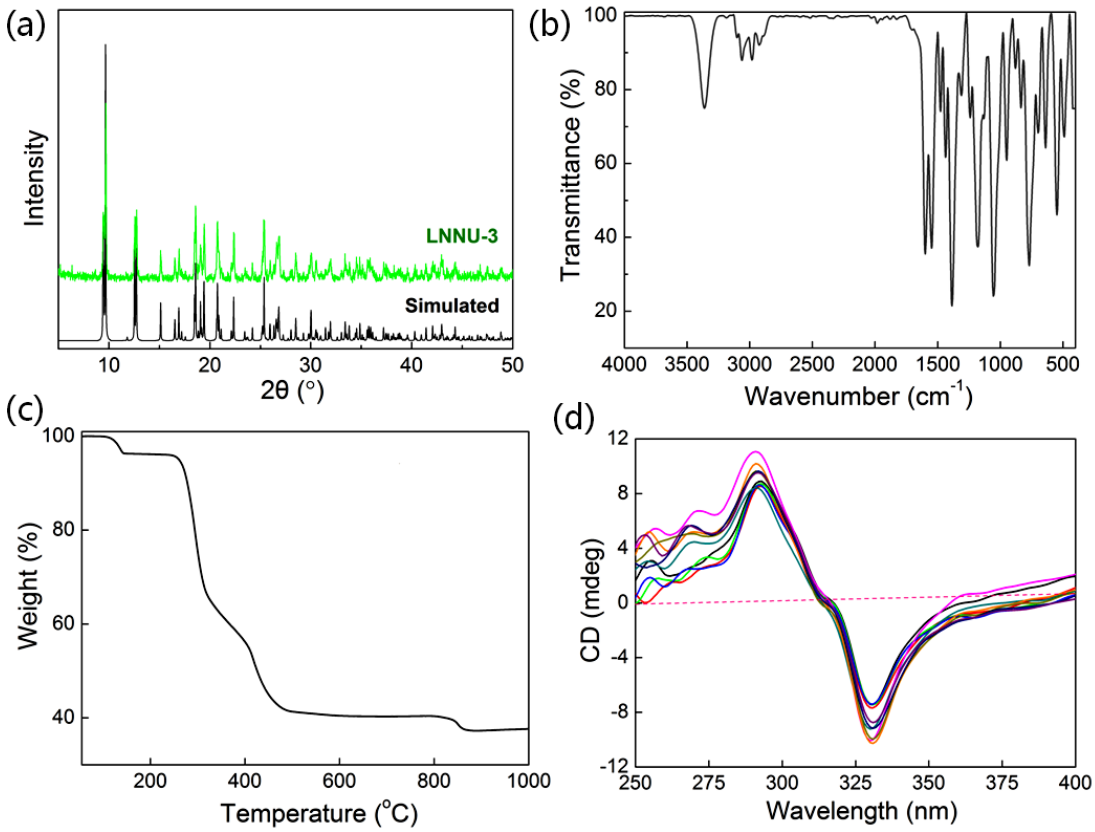

Fig. S6 (a) PXRD patterns, (b) FT–IR spectrum and (c) TG curve of **LNNU-3**; (d) Solid-state CD spectra of ten samples of **LNNU-3** were randomly picked from the same batch.

Table S5 Crystal data and structure refinement for **LNNU-3**

Formula	$C_{20}H_{21}N_2O_6PCd$
Fw	528.76
Crystal size (mm)	0.219 × 0.077 × 0.069
Crystal system	Orthorhombic
Space group	$P2_12_12_1$
a (Å)	10.4713(3)
b (Å)	10.7176(4)
c (Å)	18.7468(6)
V (Å^3)	2103.90(12)
Z	4
D_c (g cm^{-3})	1.669
μ (mm^{-1})	1.154
F (000)	1064
GOF on F^2	1.054
Unique date, R_{int}	4344, 0.0186
Theta range (º)	2.173 to 26.500
R_1, wR_2 [a)] (for I>2σ (I))	0.0193, 0.0463
R_1, wR_2 [a)] (for all data)	0.0214, 0.0471
$\Delta\rho_{max}$, $\Delta\rho_{min}$ (e Å^{-3})	0.429, –0.249
Flack parameter	0.000(9)
CCDC number	1964196

[a)] $R_1 = \Sigma (|F_0|-|F_C|) / \Sigma |F_0|$; $wR_2 = [\Sigma w (|F_0|-|F_C|)^2 / \Sigma w F_0^2]^{1/2}$

Table S6 Selected bond lengths (Å) and angles (º) for **LNNU-3**

Bond lengths (Å)			
Cd(1)–O(1)	2.200(2)	P(1)–O(1)	1.498(2)
Cd(1)–O(2)#2	2.284(2)	P(1)–O(2)	1.501(2)
Cd(1)–O(4)#1	2.212(2)	P(1)–O(3)	1.580(2)
Cd(1)–O(6)	2.533(2)	P(1)–C(1)	1.803(3)
Cd(1)–N(1)	2.366(3)	O(3)–C(9)	1.427(6)
Cd(1)–N(2)	2.331(3)	O(4)–C(8)	1.262(4)
C(9)–C(10)	1.400(11)	O(5)–C(8)	1.238(4)
Bond angles (º)			
O(2)#2Cd(1)–O(4)#1	87.92(9)	O(2)–P(1)–O(1)	117.12(14)
O(2)#2Cd(1)–O(1)	97.46(9)	O(2)–P(1)–O(3)	106.27(14)
O(4)#1–Cd(1)–O(1)	100.29(11)	O(1)–P(1)–O(3)	110.68(14)
O(2)#2–Cd(1)–N(1)	98.44(9)	O(2)–P(1)–C(1)	110.59(15)
O(4)#1–Cd(1)–N(1)	96.79(10)	O(1)–P(1)–C(1)	107.99(15)
O(1)–Cd(1)–N(1)	157.01(9)	O(3)–P(1)–C(1)	103.34(15)
N(2)–Cd(1)–N(1)	70.72(10)	C(9)–O(3)–P(1)	121.5(3)
O(2)#2–Cd(1)–N(2)	95.81(9)	P(1)–O(1)–Cd(1)	133.33(14)
O(4)#1–Cd(1)–N(2)	167.34(11)	C(15)–N(1)–Cd(1)	116.7(2)
O(1)–Cd(1)–N(2)	91.24(10)	C(20)–N(2)–Cd(1)	122.5(2)

Symmetry codes: #1 x + 1, y, z; #2 –x + 1, y + 1/2, –z + 1/2.

8. ICD effects of LNNU-2 with chiral Trp and its derivatives

Table S7 Peak position and intensity of the ICD signal generated by the interaction of L-Trp/L-Trp derivatives with **LNNU-2**

L-Trp and L-Trp derivatives		Active sites	ICD signal peak position (nm)	ICD signal Intensity (mdeg)
L-Trp	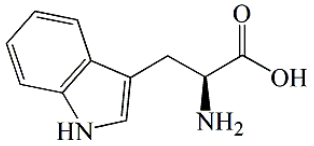	–NH_2 (1) –COOH (1) Indole group (1)	329	152.5
L-TrpNH_2	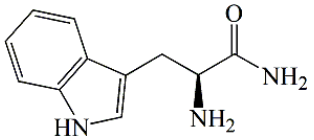	–NH_2 (1) –$CONH_2$ (1) Indole group (1)	326	117.3
L-TrpOMe	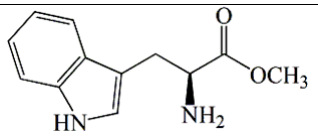	–NH_2 (1) Indole group (1)	325	61.5
*N*Ac-L-Trp	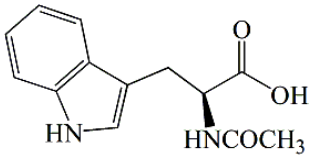	–COOH (1) Indole group (1)	——	——

9. Determination of L-Trp concentration

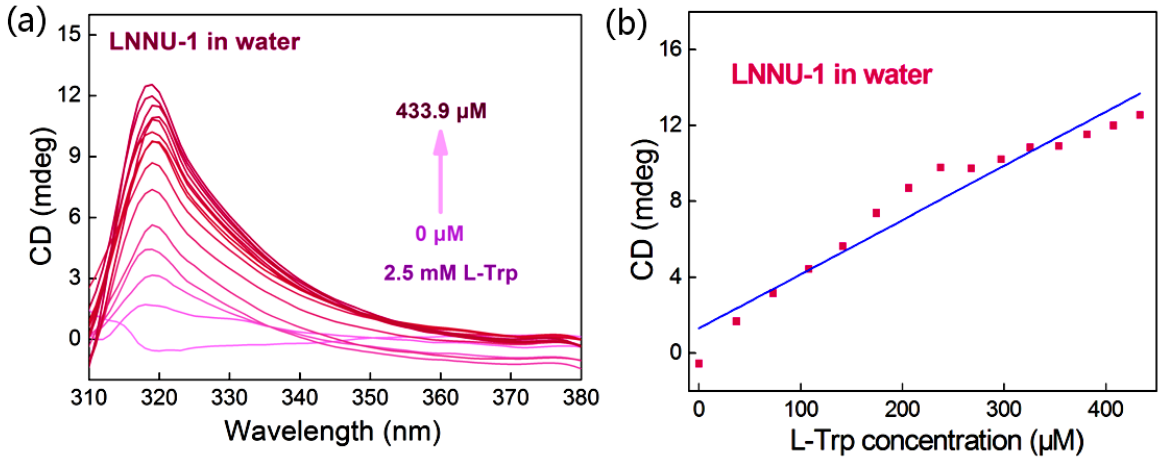

Fig. S7 (a) CD spectra of **LNNU-1** dispersed in water upon incremental addition of the aqueous solutions of L-Trp (2.5×10^{-3} M); (b) The relationship between ICD intensities at 319 nm and the concentrations of L-Trp samples.

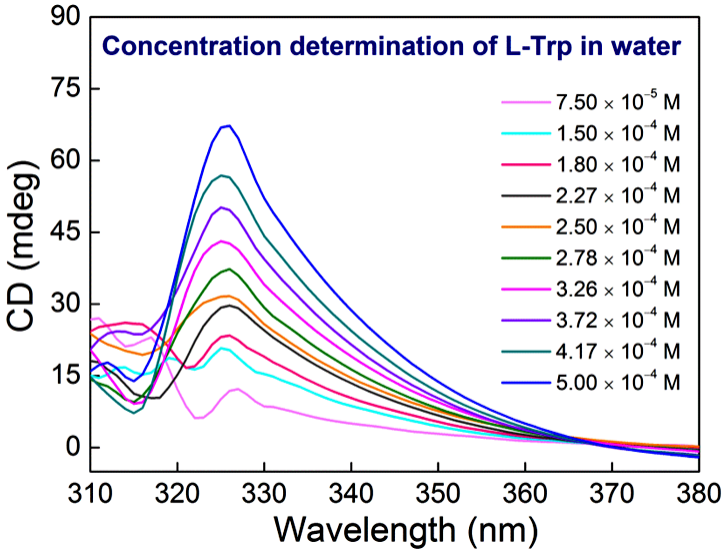

Fig. S8 CD spectra of 10 samples with varying concentrations of L-Trp in water were determined by **LNNU-2**.

Table S8 Concentration determination of L-Trp aqueous solution samples

In water			Sensing results	
Entry	Concentration (M)	ICD signal intensity (mdeg)	Concentration (M)	Relative Error (%)
1	7.50×10^{-5}	10.1681	7.83×10^{-5}	4.4
2	1.50×10^{-4}	20.7553	1.58×10^{-4}	5.3
3	1.80×10^{-4}	23.1452	1.77×10^{-4}	1.7
4	2.27×10^{-4}	29.2665	2.23×10^{-4}	1.8
5	2.50×10^{-4}	31.5543	2.40×10^{-4}	4.0
6	2.78×10^{-4}	36.6905	2.79×10^{-4}	0.4
7	3.26×10^{-4}	43.1406	3.28×10^{-4}	0.6
8	3.72×10^{-4}	50.1735	3.81×10^{-4}	2.4
9	4.17×10^{-4}	56.8697	4.32×10^{-4}	3.6
10	5.00×10^{-4}	66.8843	5.07×10^{-4}	1.4
In a mixture of 19 natural amino acids			Sensing results	
Entry	Concentration (M)	ICD signal intensity (mdeg)	Concentration (M)	Relative Error (%)
1	2.58×10^{-4}	32.7205	2.54×10^{-4}	1.6
2	2.78×10^{-4}	35.6686	2.81×10^{-4}	1.1
3	3.54×10^{-4}	43.7826	3.55×10^{-4}	0.3
4	3.99×10^{-4}	48.1946	3.96×10^{-4}	0.8
5	4.42×10^{-4}	52.9328	4.39×10^{-4}	0.7
6	4.59×10^{-4}	54.8059	4.56×10^{-4}	0.7
7	5.00×10^{-4}	59.7985	5.01×10^{-4}	0.2
8	5.54×10^{-4}	65.5011	5.53×10^{-4}	0.2
9	6.06×10^{-4}	70.8963	6.02×10^{-4}	0.7
10	6.82×10^{-4}	79.4394	6.80×10^{-4}	0.3
In simulated blood plasma components			Sensing results	
Entry	Concentration (M)	ICD signal intensity (mdeg)	Concentration (M)	Relative Error (%)
1	1.42×10^{-4}	22.4446	1.47×10^{-4}	3.5
2	1.85×10^{-4}	27.0059	1.85×10^{-4}	0
3	2.68×10^{-4}	37.0720	2.70×10^{-4}	0.7
4	3.81×10^{-4}	50.9574	3.86×10^{-4}	1.3
5	4.76×10^{-4}	62.4806	4.82×10^{-4}	1.3
6	5.54×10^{-4}	71.3548	5.56×10^{-4}	0.4
7	6.06×10^{-4}	77.4476	6.07×10^{-4}	0.2
8	6.88×10^{-4}	86.8851	6.86×10^{-4}	0.3
9	7.46×10^{-4}	94.0277	7.46×10^{-4}	0
10	8.05×10^{-4}	101.1990	8.06×10^{-4}	0.1

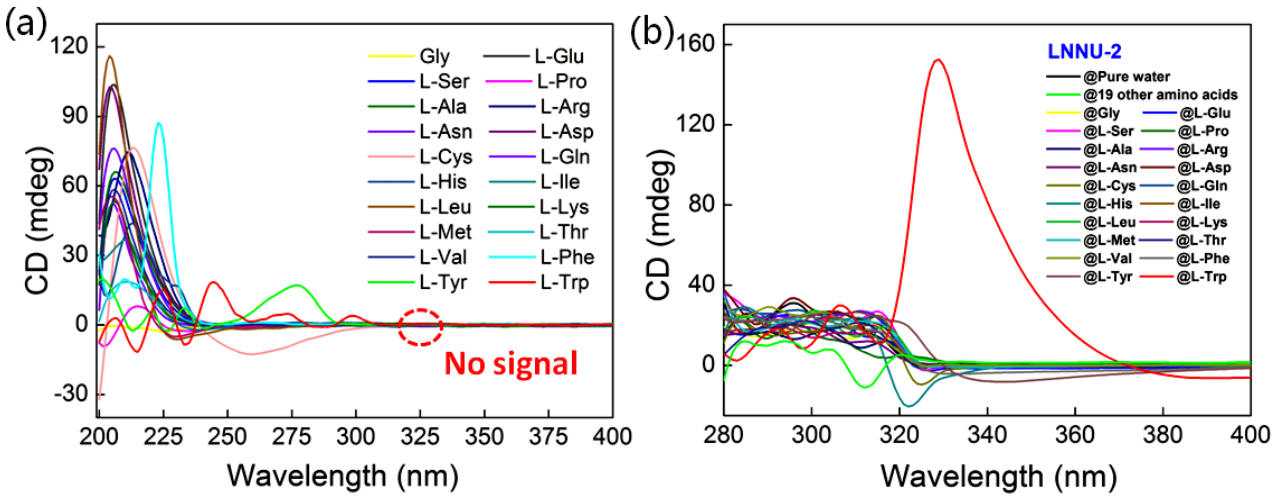

Fig. S9 (a) CD spectra of the pure aqueous solutions of all natural amino acids (2.5×10^{-3} M); (b) CD spectra of **LNNU-2** dispersed in pure water, the aqueous solutions of all natural amino acids and a mixed aqueous solution of 19 other natural amino acids, respectively.

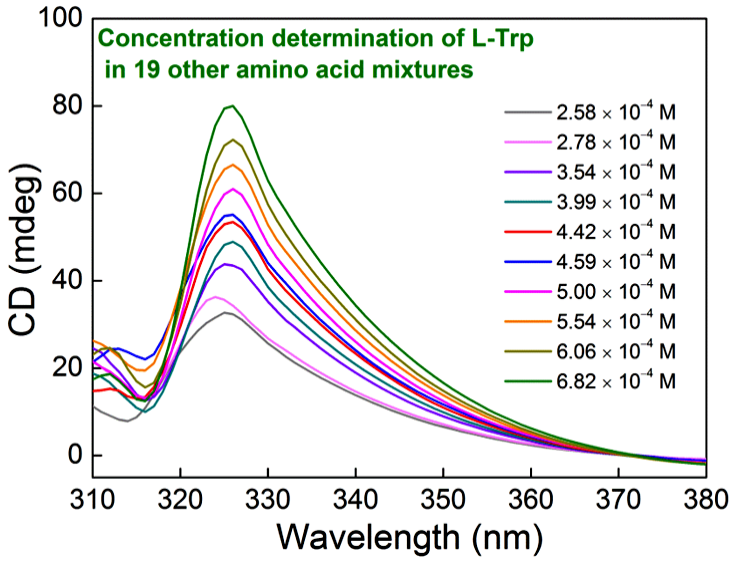

Fig. S10 CD spectra of 10 samples with varying concentrations of L-Trp in the mixed aqueous solution of 19 other natural amino acids were determined by **LNNU-2**.

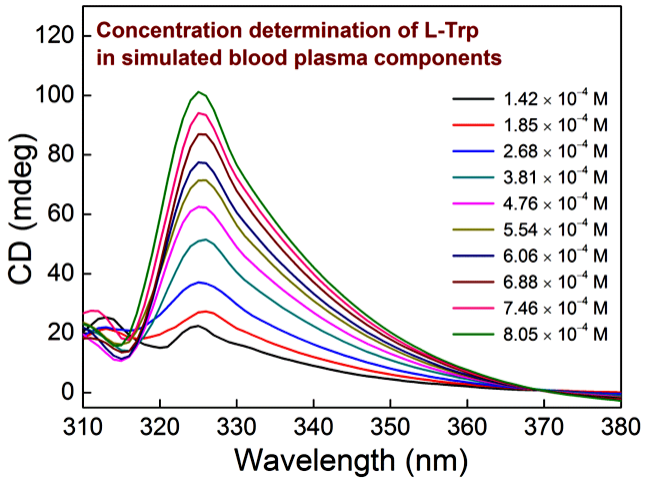

Fig. S11 CD spectra of 10 samples with varying concentrations of L-Trp in the mixed aqueous solution of blood plasma components were determined by **LNNU-2**.

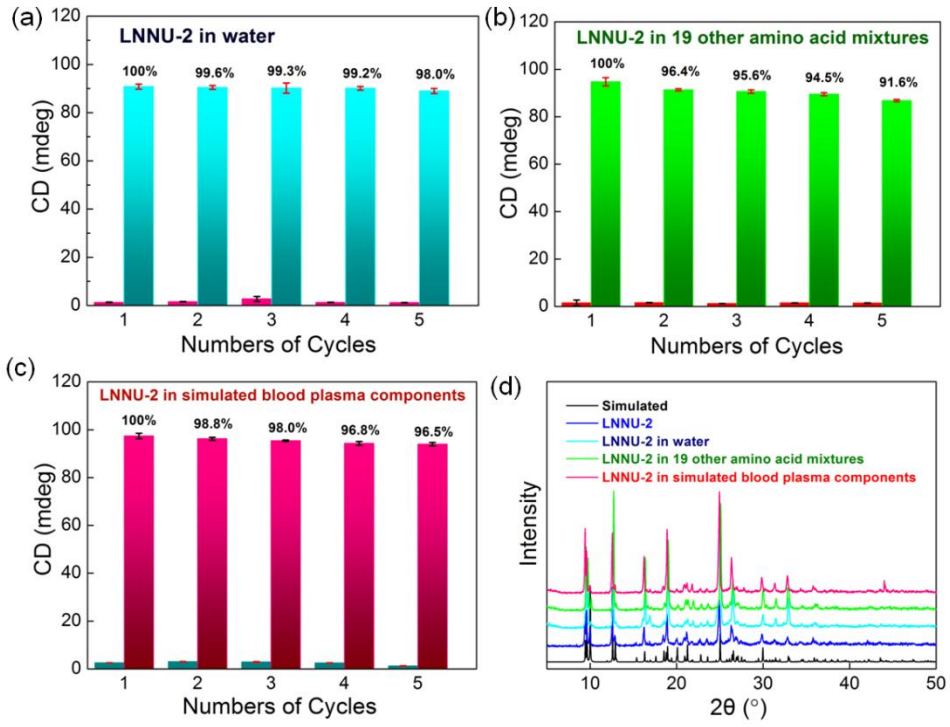

Fig. S12 The recyclable study of **LNNU-2** dispersed in water (a), mixed natural amino acids (b) and simulated blood plasma components (c) in the presence of L-Trp with five continuous cycles (the magenta/red/dark cyan bars represent the initial ICD signal intensity and the cyan/green/pink bars represent the ICD signal intensity upon addition an aqueous solution of L-Trp; (d) PXRD patterns of **LNNU-2**; the simulated, as-synthesized product, and the samples after five cycle tests of **LNNU-2** sensing L-Trp in water, mixed natural amino acids and simulated blood plasma components.

10. Determination of the enantiomeric composition of chiral Trp and chiral aromatic amino alcohols

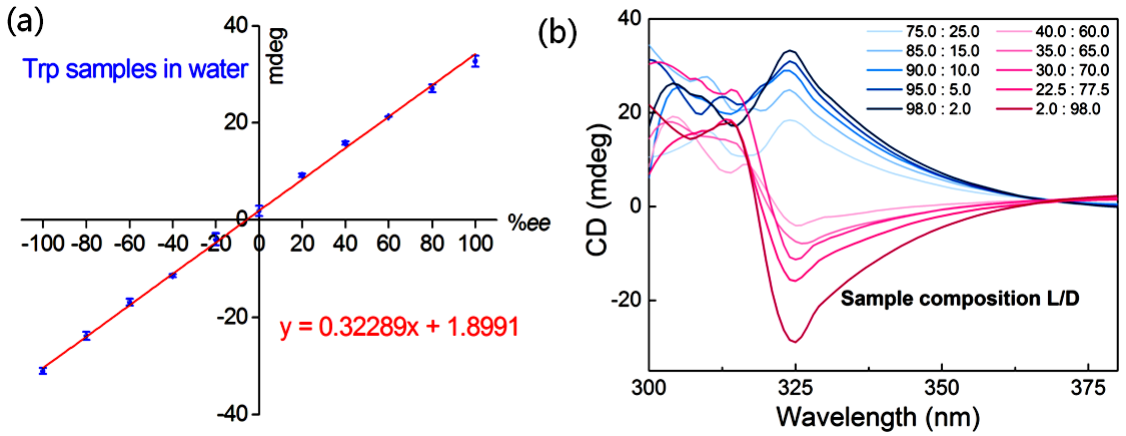

Fig. S13 (a) Plot of the ICD signal intensities at 325 nm versus *ee* values of the Trp samples; (b) CD spectra of 10 Trp samples with varying enantiomeric composition were determined by **LNNU-2**.

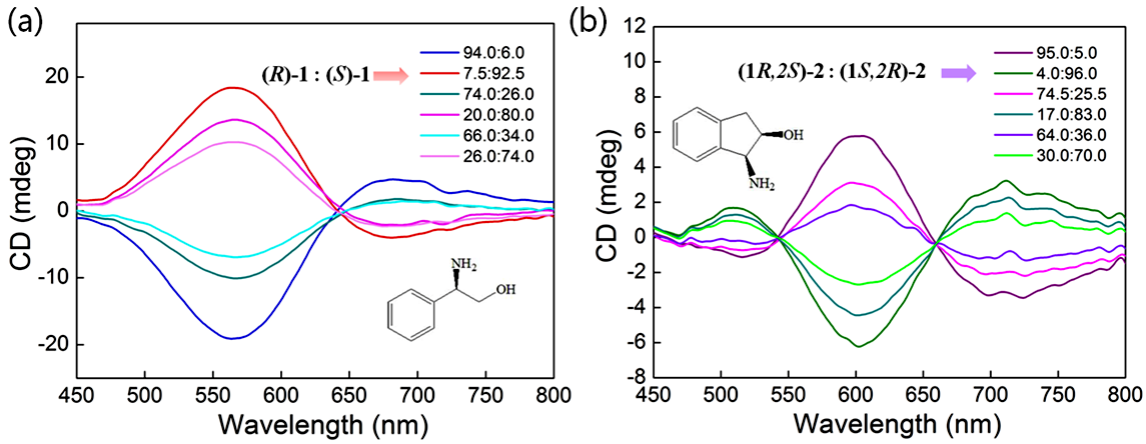

Fig. S14 (a) CD spectra of six 2-phenylglycinol (**1**) samples with varying enantiomeric composition in pure water were determined by **LNNU-2**; (b) CD spectra of six (–)-cis-1-amino-2-indanol (**2**) samples with varying enantiomeric composition in pure water were determined by **LNNU-2**.

11. Chiral induction synthesis of enantioenriched LNNU-2

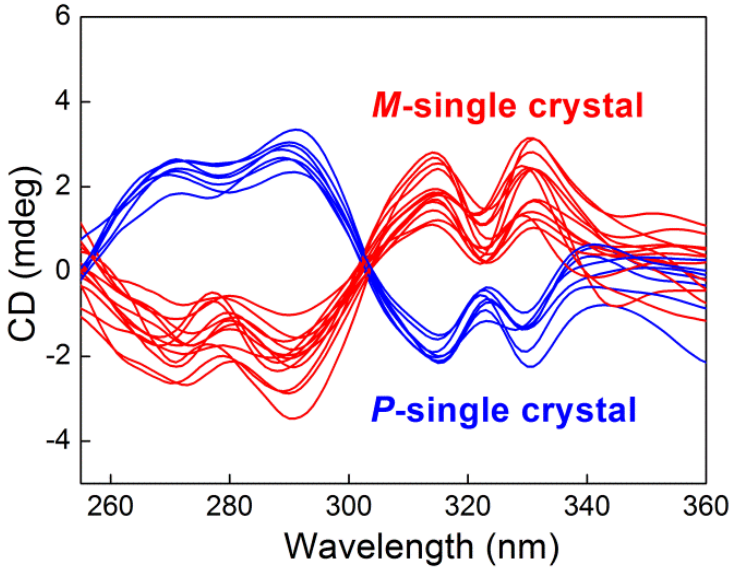

Fig. S15 Solid-state CD spectra of 20 single crystal sample of **LNNU-2** were randomly picked from the same batch.

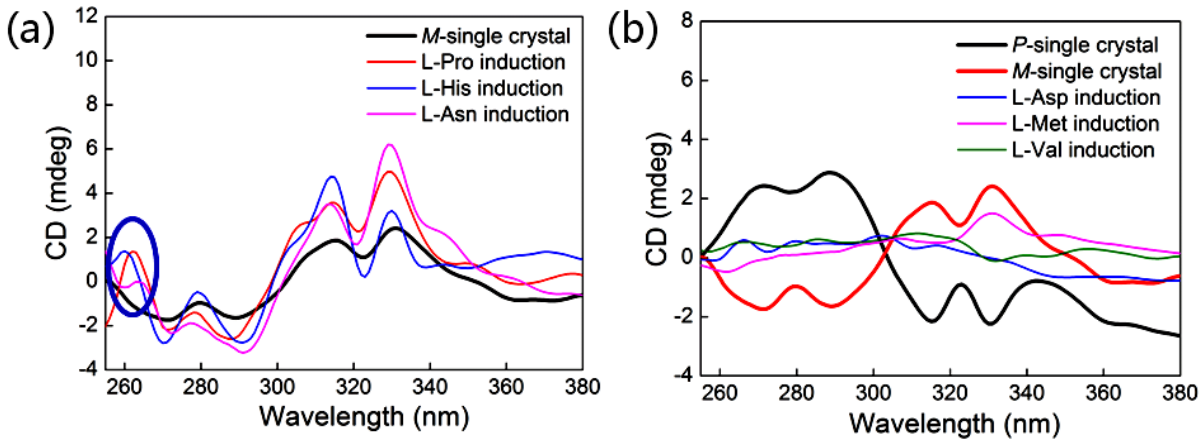

Fig. S16 Solid-state CD spectra of the products induced by chiral amino acids.

Table S9 The synthesis results of **LNNU-2** induced by chiral amino acids

Chiral amino acid	Molecular structure of chiral amino acid	Type of chiral amino acid	Yield of LNNU-2 products (based on H_2L)	Chiral feature of LNNU-2 products
L-Trp	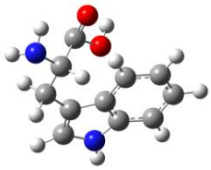	Aromatic	72.0%	Racemic
D-Trp			66.8%	Racemic
L-Pro	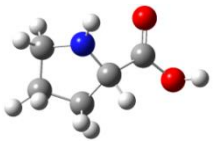	Sub-amino acids	62.2%	enantiomeric excess (*M*)
L-His	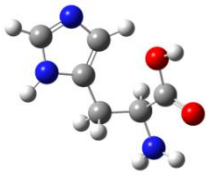	Alkaline	75.4%	enantiomeric excess (*M*)
L-Asp	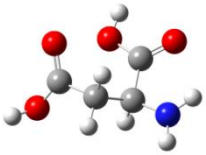	Acidic	63.8%	Racemic
L-Asn	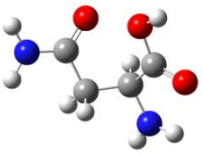	Amides	61.4%	enantiomeric excess (*M*)
L-Met	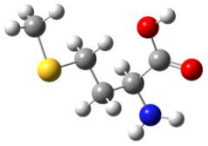	Sulfur containing	36.8%	Racemic
L-Val	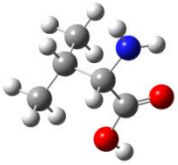	Aliphatic	41.7%	Racemic
L-Ala	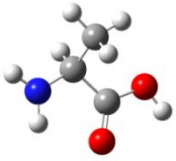	Aliphatic	44.6%	Enantioenriched (*P*)
D-Ala			59.8%	Enantioenriched (*M*)

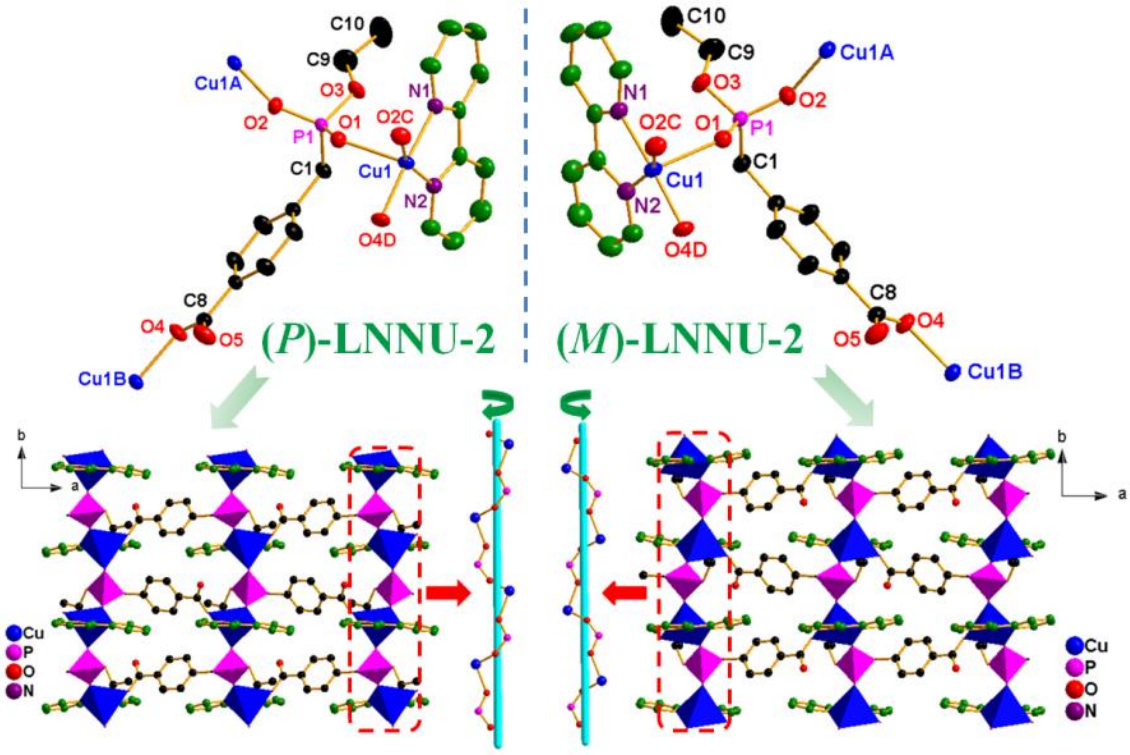

Fig. S17 Crystal structures of **LNNU-2** enantiomers.

Table S10 Crystal data and structure refinement for **(*P*)-LNNU-2**

Formula	$C_{20}H_{21}N_2O_6PCu$
Fw	479.90
Crystal size (mm)	0.883 × 0.743 × 0.592
Crystal system	Orthorhombic
Space group	$P2_12_12_1$
a (Å)	10.0728(9)
b (Å)	10.8716(10)
c (Å)	18.3600(17)
V (Å^3)	2010.6(3)
Z	4
D_c (g cm^{-3})	1.585
μ (mm^{-1})	1.207
F (000)	988
GOF on F^2	1.005
Unique date, R_{int}	3682, 0.0200
Theta range (º)	2.177 to 25.497
R_1, wR_2 [a)] (for $I>2\sigma(I)$)	0.0220, 0.0587
R_1, wR_2 [a)] (for all data)	0.0229, 0.0591
$\Delta\rho_{max}$, $\Delta\rho_{min}$ (e Å^{-3})	0.243, –0.390
Flack parameter	0.025(4)
CCDC number	1964192

[a)] $R_1 = \Sigma(|F_0|-|F_C|)/\Sigma|F_0|$; $wR_2 = [\Sigma w(|F_0|-|F_C|)^2/\Sigma w F_0^2]^{1/2}$

Table S11 Selected bond lengths (Å) and angles (º) for **(*P*)-LNNU-2**

Bond lengths (Å)			
Cu(1)–O(1)	2.2802(18)	P(1)–O(1)	1.4889(19)
Cu(1)–O(2)#1	1.932(2)	P(1)–O(2)	1.4977(19)
Cu(1)–O(4)#2	1.9428(19)	P(1)–O(3)	1.588(2)
Cu(1)–N(1)	2.010(2)	P(1)–C(1)	1.812(3)
Cu(1)–N(2)	2.041(2)	O(3)–C(9)	1.447(4)
C(9)–C(10)	1.414(10)	O(4)–C(8)	1.274(4)
O(5)–C(8)	1.235(4)		
Bond angles (º)			
O(2)#1–Cu(1)–O(4)#2	94.22(9)	O(1)–P(1)–O(2)	118.18(11)
O(2)#1–Cu(1)–O(1)	96.31(8)	O(2)–P(1)–O(3)	110.35(12)
O(4)#2–Cu(1)–O(1)	90.15(8)	O(1)–P(1)–O(3)	106.73(11)
O(2)#1–Cu(1)–N(1)	90.00(10)	O(1)–P(1)–C(1)	110.97(13)
O(4)#2–Cu(1)–N(1)	175.34(9)	O(2)–P(1)–C(1)	106.06(13)
O(1)–Cu(1)–N(1)	91.37(8)	O(3)–P(1)–C(1)	103.62(12)
N(1)–Cu(1)–N(2)	79.84(10)	C(9)–O(3)–P(1)	121.0(2)
O(2)#1–Cu(1)–N(2)	160.60(9)	P(1)–O(1)–Cu(1)	133.77(11)
O(4)#2–Cu(1)–N(2)	95.55(9)	C(15)–N(1)–Cu(1)	116.15(19)
O(1)–Cu(1)–N(2)	100.37(8)	C(20)–N(2)–Cu(1)	126.6(2)

Symmetry codes: #1 –x + 2, y + 1/2, –z + 1/2; #2 –x + 1, y + 1/2, –z + 1/2.

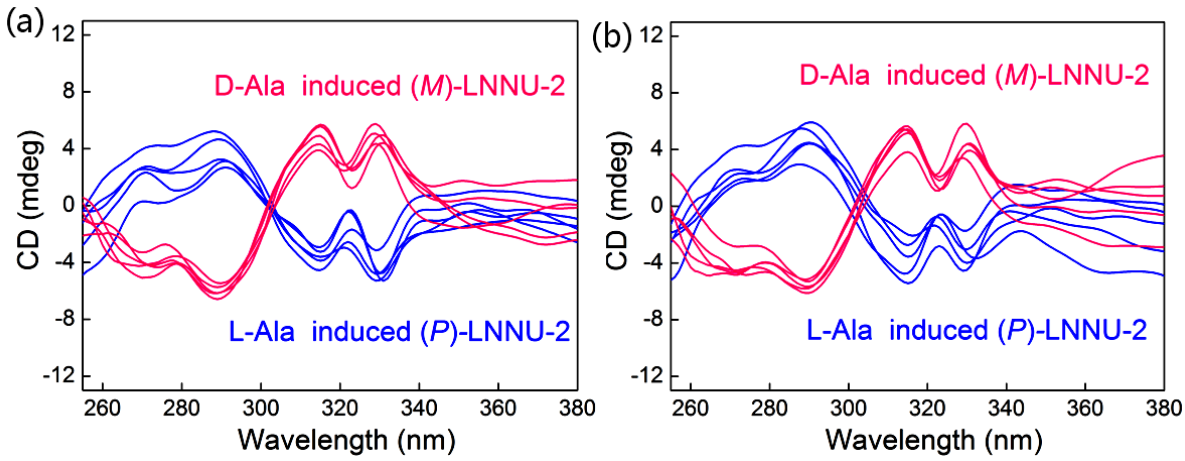

Fig. S18 Solid-state CD spectra of the samples induced by L-Ala/D-Ala were randomly picked from two parallel batches.

12. References

1. Y.-F. Liu, G.-F. Hou, Y.-H. Yu, P.-F. Yan, J.-Y. Li, G.-M. Li and J.-S. Gao, pH-Dependent Syntheses, Luminescent, and Magnetic Properties of Two-Dimensional Framework Lanthanide Carboxyarylphosphonate Complexes, *Cryst. Growth Des.*, 2013, **13**, 3816–3824.
2. G. M. Sheldrick, Crystal Structure Refinement with SHELXL, *Acta Crystallogr. C Struct. Chem.*, 2015, **71**, 3–8.
3. Y.-Y. Zhu, Y.-N. Zhou, X. Zhang, Z.-G. Sun and C.-Q. Jiao, Homochiral MOF as Chiroptical Sensor for Determination of Absolute Configuration and Enantiomeric Ratio of Chiral Tryptophan, *Adv. Opt. Mater.*, 2021, **9**, 2001889.
4. H. D. Flack and G. Bernardinelli, The Use of X-ray Crystallography to Determine Absolute Configuration, *Chirality*, 2008, **20**, 681–690.